ASTRONOMY & ASTROPHYSICS
SUPPLEMENT SERIES

Astron. Astrophys. Suppl. Ser. **113,** 399-408 (1995)

Automatic selection of new Hα emission-line galaxies using MAMA*

O. Alonso, J. Zamorano, M. Rego and J. Gallego

Depto. Astrofísica, Facultad de CC Físicas, Universidad Complutense de Madrid, E-28040 Madrid, Spain

Received September 27, 1994; accepted March 18, 1995

Abstract. — A full set of algorithms for the automatic analysis of low-resolution objective-prism spectra has been developed with the aim of finding new emission-line galaxies (ELGs) candidates from the Universidad Complutense de Madrid (UCM) survey prism plates. An objective-prism plate and a direct plate, used for pairing objects and to perform star-galaxy separation, have been scanned with the MAMA machine. The plates were taken in the red region of the spectrum, using the Hα+[NII] blend in emission as selection criterion. The procedure, applied to digitized spectra, is able to automatically select ELGs candidates. Density to intensity transformation has not been used in our method; the detection of the emission is performed applying three independent criteria over the one-dimensional spectra in raw data. The automatically selected sample is compared with that obtained after a careful visual scan. Spectroscopic observations at moderate spectral resolution are presented for the whole sample of candidates in order to study the drawbacks and the biases of both methods.

Key words: methods: data analysis — techniques: image processing — surveys — galaxies: general

1. Introduction

The photographic plate is a powerful tool, still essential in several astronomical works needed to cover wide areas of the sky and to study a great number of objects in selected fields, both to analyze their global properties and to search for a certain kind of objects (West 1991; Lipovetsky 1994). Nevertheless, the main problem becomes the large amount of data recorded on a single exposure, covering a typical field 5° wide in Schmidt photographic plates. The development of fast and high performance automated measuring machines has allowed to extract all the stored information and process it in a short period of time. In addition, the use of such devices provides accurate quantitative results not dependent on subjective criteria.

A Schmidt-type telescope, equipped with an objective prism, allows not only to examine a large field, but also to obtain very low dispersion spectra for all the objects. This technique is used in searches for objects with peculiar spectral features and in spectral classification programs. Slitless spectroscopy has proven to be an efficient technique for conducting quasars and emission-line galaxies surveys. Although several surveys of ELGs have been carried out with different techniques and selection criteria (see excellent reviews in Kinman 1984 and Véron 1986), either searching for objects with unusual colors in multiexposure plates (Haro 1956; Takase & Miyauchi-Isobe 1993 and references therein) or with anomalous UV excess in prism plates as was done by Markarian (1967), the most direct way to undertake these searches is directly by looking for objects showing the emission-line features in prism plates of adequate dispersion (Smith 1975; MacAlpine & Williams 1981; Kinman 1984; Markarian 1987; Maza et al. 1989). Surveys like these have been developed in the past mainly using the blue region of the spectrum, where photographic emulsions were more sensitive, and looking for objects with strong emission lines as [OII]λ3727 Å, Hβ or [OIII]$\lambda\lambda$4959,5007 Å.

However, surveys in the blue can miss a significant number of ELGs due to strong extinction, low excitation (Kinman 1984; Gallego 1995) or extreme metal-poor abundance (Kunth & Sargent 1986; Boroson et al. 1993) because of the weakness of [OIII] lines. Surveys looking for the Hα line in emission can solve this problem. The Second Byurakan Spectral Sky Survey (Markarian et al. 1987) uses three different spectral ranges (blue, green and red) to identify different types of objects and shows that more than 50% of the candidates of the survey are selected in the red region. In addition, objective-prism searches

Send offprint requests to: J. Zamorano

*MAMA (Machine Automatique à Mesurer pour l'Astronomie) is developed and operated by CNRS/INSU (Institut National des Sciences de l'Univers) and located at the Observatoire de Paris

in Hα are a powerful observational tool in works concerning the study of star formation in galaxies (Moss & Whittle 1993) since the global Hα+[NII] emission is a good and direct measurement of current massive star formation (Kennicutt & Kent 1983; Kennicutt 1992). The number of surveys in the red has increased recently due to the improvement in plate sensitivity in the red region of the spectrum (Kinman 1984; Wamsteker et al. 1985; Markarian et al. 1987; Moss & Whittle 1988; Zamorano et al. 1994).

In the past, the search of ELGs and QSOs with objective prism plates, looking for spectra showing emission-line features, was carried out visually, but the subjective criteria of the selection could derive biased samples and produce observer-dependent systematic effects in the final results. Much effort has been put into improving the extraction of information from photographic plates by means of fast scanning microdensitometers and into the data analysis (Clowes et al. 1980; Borra et al. 1987, 1988; Edwards et al. 1988), although most of the searches of ELGs are still performed by visual scan (Moss et al. 1988; Surace & Comte 1994; Zamorano et al. 1994).

We have undertaken a new program for automatic identification of emission-line galaxies in the UCM survey (Rego et al. 1989; Zamorano et al. 1990, 1994) using the MAMA machine. This paper presents the specific algorithms developed and the first results obtained with two digitized plates. In the next section we describe the photographic material and the digitization characteristics. In Sects. 3 and 4 we explain the algorithms developed for the data reduction and the criteria applied for the selection of the candidate sample of ELGs. In Sect. 5 our results are compared with those obtained in the visual search. Finally, in Sect. 6 we present spectroscopic observations and we specially analyze the objects lost by both the visual and the automatic searches.

2. Plate material and digitization

2.1. *Plate material*

Two plates from the UCM objective-prism survey, not previously analyzed, have been used to carry out this work. Direct and objective-prism plates were taken with the 80/120 cm $f/3$ Schmidt Telescope of the Calar Alto German-Spanish Observatory in Almería, Spain (Birkle 1984). Full details of plates are listed in Table 1. The IIIa-F Kodak plates were hypersensitized by baking them in a forming-gas atmosphere at 65°C during two hours before exposure. The telescope plate scale of 86″/mm allows to cover a field of 5.°5×5.°5 in 24×24 cm^2 plates. The use of IIIa-F emulsion, with a sharp red cut-off at 6850 Å, and RG630 filter provides a useful spectral range from 6400 to 6850 Å. A full aperture 4° objective-prism, applied to obtain the prism plate, gives a dispersion of 1950 Å/mm at Hα along the N-S axis. The typical size of the spectra is ≈ 0.4 mm and, therefore, the overlapping is not very frequent. The spectra were not widened in order to achieve a maximum sensitivity. This instrumental set-up allows to register the Hα+[NII][1] lines in emission for objects up to $z = 0.04$. A detailed explanation of the instrumental and observational procedure can be consulted in Zamorano et al. (1994).

Table 1. Plate material

	A384 (Direct plate)	A335 (Prism plate)
R.A. (2000.0)	$15^h\ 00^m\ 46.^s7$	$15^h\ 00^m\ 03.^s5$
DEC (2000.0)	28° 35′ 29″	27° 52′ 33″
Emulsion	IIIa-F	IIIa-F
Filter	RG630	RG630
Exp. time	45 min	120 min
Prism	–	4°
Field	5.°5×5.°5	5.°5×5.°5
Plate size	24×24 cm^2	24×24 cm^2
Dispersion	–	1950 Å/mm
Plate Scale	86″/mm	86″/mm
Date	15 FEB 91	26 JUN 90

The instrumental setup imposes the use of different guide stars for the acquisition of direct and prism plates, so the registered fields are not exactly the same. The common area represent the 85% of the whole plate and the subsequent work will be restricted to it.

2.2. *Plate digitization*

Direct and objective-prism plates were digitized in December 1992 by the MAMA machine (Guibert & Moreau 1991; Moreau 1992) at the Observatoire de Paris. MAMA is a high speed multichannel microdensitometer with high photometric and positional accuracy, able to scan a full photographic plate in a few hours. A pixel size and sampling step of 10 μm, the higher resolution achieved by the machine, was used, following the standard procedure elaborated and tested by the support staff.

Before plate scanning, we follow a standard procedure in order to derive the plate constants which enables us to transform between the X, Y coordinates measured on the plate and the celestial coordinates (α,δ). A third-order polynomial transformation is derived by using astrometric reference stars from the PPM catalog (Roeser & Bastian 1991). Although a full plate astrometric reduction does not achieve high accuracy (Taff et al. 1990), such precision is not needed in this study, and errors up to 1 arcsec are accepted. In fact, the rms in the residua of the astrometric reduction are 0.″29 and 0.″33 for direct and prism plate respectively.

[1]The combined Hα+[NII] emission will be referred to in what follows as simply the Hα emission.

The plates were scanned using two different modes of operation. In the first scan, (*ZONE* mode) the machine processes the data in real time and detects the objects by thresholding the image a certain number of sigma above the plate background. Several parameters are calculated for all the objects with a minimum size in pixels. This value must be small to include the faintest objects but large enough to reject the high number of spurious identifications. A value of 10 and 15 pixels for objects in direct and prism plates respectively were used. A catalog containing several parameters for all images, as position, density flux, area, semiaxis and position angle, second moment orders, sky density and others, is finally created and stored on magnetic tape. The prism plate was scanned again using the *IMAGE* mode, in which the machine measures the raw photographic density of each plate pixel, creating a large number of images in FITS format. This mode of digitization produces a high volume of data. For example, the 24×24 cm^2 plate with a 10 μm pixel size returns around 1 Gbyte of information.

3. Data analysis

In this work, we intend to select all the spectra showing emission-line features in an objective prism plate via automatic analysis. The Hα line in emission is clearly visible in density as proved by the success of several searches performed in the pass by visual scanning. Consequently, the ELG candidates could be easily recognized in the digitized spectra without transforming density to intensity values. In addition, no calibration spots were exposed on the plates during the acquisition to derive the characteristic curve. Therefore, all the analysis has been performed in density, in fact, in instrumental MAMA density ($d_{\rm M}$), related with photographic density ($d_{\rm Ph}$) by

$$d_{\rm M} = \frac{4095}{\log 4095} d_{\rm Ph} \qquad (1)$$

where $d_{\rm M}$ takes integer values in the range 0–4095 (Moreau 1992). Nearly all the objects in a wide-field photographic plate are stars and normal galaxies. ELGs will be selected then to show significant deviations from "normal" spectra.

3.1. *Spurious object rejection and star-galaxy separation*

During the ZONE scan mode, MAMA includes in the catalogue not only the real images, but also emulsion flaws, plate scratches and satellite tracks. A first step must be done to reject the spurious detection. The majority of them can be recognized with an analysis of the object shape, but a complex algorithm must be developed in order to preserve extended and peculiar spectra. The parameters given by the measuring machines during the plate scan can be used to classify the objects and to separate between emulsion scratches, stars and galaxies (Jarvis & Tyson 1981; Borra et al. 1987; Infante & Pritchet 1992). But the most direct way to reject spurious detection consists in comparing two different plates of the same field, that is, searching each object from one plate into the other, and retaining only the paired data.

A special analysis must be done because we intend to pair a direct and a prism plate. When we try to process two direct plates, a star on one plate can be searched inside a small circle of 2 or 3 arcsec, centered in the coordinates derived from the position measured on the other plate. In our case, we are working with a prism plate, where the images are elongated towards the dispersion direction. This allows large deviations between the position in direct and prism plate because of the variation of length of the prism image with the object brightness. The use of a circular search area is not a good choice, and we must permit large deviations in the dispersion direction. Finally, we select a box of 5×2 arcsec to pair the objects. Figure 1 shows the positional residua of the 19 658 objects selected as final result.

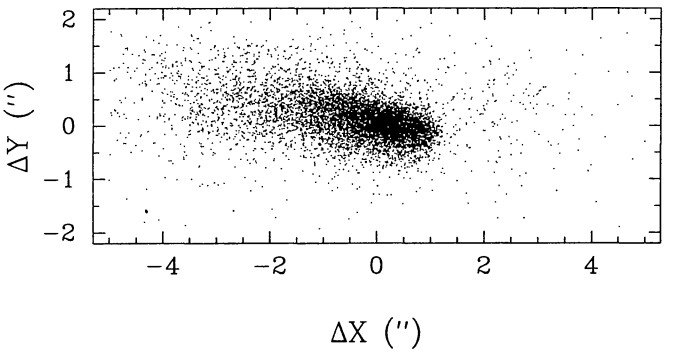

Fig. 1. Final residua of the pairing process between direct and prism plate using a search box of 5″ × 2″

The parameters given by MAMA for the direct plate can be used to perform a star-galaxy separation. A large number of works has been undertaken in this way, and several properties must be studied in order to assure a precise star-galaxy discriminator algorithm (Odewahn et al. 1993; Schuecker 1993; Infante & Pritchet 1992). Although the stellar-like objects could not be excluded of the rest of the procedure in order to retain possible very compact emission-line galaxies, a separation of extended objects can help us facilitating the selection task. On the one hand, one expects to obtain very few ELG candidates in the stellar sample, and this can be used as test in the programs. On the other hand, the extended objects need a more detailed analysis because the Hα visibility depends on several factors such as the spatial distribution of the emission, the surface brightness or the apparent size, shape and orientation of the galaxy.

We have used a plot of the logarithm of the area versus density flux to discern between stellar-like and extended objects (Reid & Gilmore 1982). As shown in Fig. 2, the

plot presents a bimodal distribution, with the majority of the points concerning stellar objects and located following a general tendency. Galaxies and extended objects, with lower surface brightness, present lower density fluxes for a given area. We have used an iterative method, fitting a spline curve to the data and rejecting points with large deviations. In each step, the curve comes nearer to the stellar sequence. Figure 2 shows the final fit together with the 3σ threshold, used to segregate the galaxies.

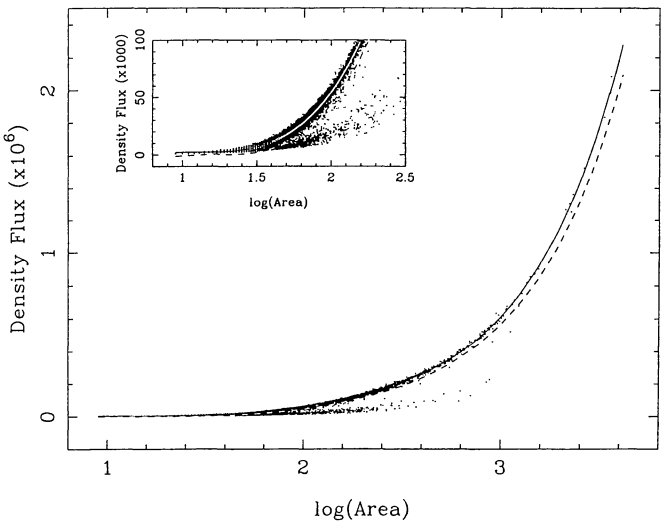

Fig. 2. Density flux versus log area plot used to discriminate between stellar and extended objects. Solid line shows the curve fitted to general sequence concerning to stellar data. The dashed line shows the 3σ curve used to segregate galaxies

3.2. *Spectra extraction*

The majority of the pixels returned after the plate scan belong to sky background, and do not offer relevant information. Moreover, the background density is automatically measured by MAMA during the ZONE digitization and given for each object in the created catalogues. In order to reduce the volume of data to be analyzed, a box of 61×21 pixels ($52''\times18''$) was extracted around each object creating mosaic images. The box size is large enough to include bright and extended objects. All the spectra, that is, all the needed information, can be stored in 50 Mbyte after the process, allowing a fast and easier access to the data.

The one-dimensional spectra were extracted using marginal sums perpendicular to the direction of the dispersion. Only the 5 central scans, those with higher signal, were used in order to achieve a high signal without increasing the noise. We have summed the density values of each pixel, giving the spectra in arbitrary density units. Optimal spectrum extraction algorithms as given by Hewett et al. (1985) and Horne (1986) have been applied and tested, but the small improvement in the results does not justify the high increase of processing time.

3.3. *Continuum fit*

The prism spectra are totally dominated by the instrumental emulsion+filter response due to the reduced spectral range (6400–6850 Å), and the low dispersion provided by the prism. Only the sharp red cut-off of the IIIa-F emulsion offers a weak reference point for wavelength calibration, although it depends on magnitude and color. The Hα line in emission is the only real spectral feature we can see in prism spectra, but its position varies in general with redshift and spatial shape for very extended objects. However, one expects to have an excess in the signal over the instrumental profile if the object presents the Hα line in emission. An approach to identify this type of objects consists in determining the continuum shape of the spectra and to look for objects with large residuals over the estimated continua.

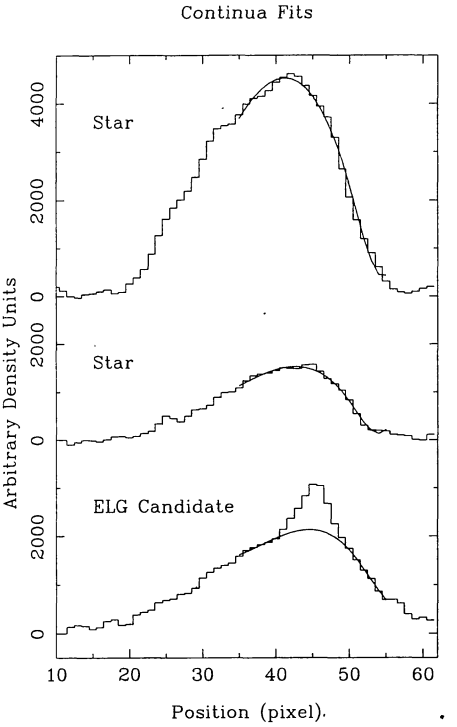

Fig. 3. Examples of the continuum fit procedure applied to different objects. The stellar spectra can be modeled by a continuum, whereas the ELG prism spectrum shows a significant residuum

The first step consists in locating the sharp IIIa-F emulsion red cut-off for all the objects, using the minimum of the C_j function defined by Borra et al. (1987) as a cut-off finder,

$$C_j = \sum_{i=j+\frac{b+1}{2}}^{j+a+\frac{b-1}{2}} S_i - \sum_{i=j-a-\frac{b-1}{2}}^{j-\frac{b+1}{2}} S_i \qquad (2)$$

The C_j function is evaluated in each point as the difference between the sum of the density values of the spectrum (S_i) within two windows symmetric to pixel j, having a pixels width and distant b pixels. We have tested that the values of $a = 5$, $b = 1$ provide the best results. This does not allow an accurate wavelength calibration, but the knowledge of the point in which the prism spectrum abruptly drops is essential for the subsequent fit of the continuum.

The use of density units and the different spectral distribution of all the objects does not allow to obtain a continuum pattern to be scaled and fitted to each spectrum. It is necessary to create a curve able to fit all type of spectra, but it also must point out the emission feature if this one exists. With this aim, a cubic spline curve was fitted from central to red region of the spectrum, the range where we will search for the line. An iterative process has been adopted, rejecting points 2 sigma over the calculated continuum. This procedure provides accurate continua for all the spectral shapes, including those with a strong emission line feature, as we show in Fig. 3.

3.4. *Analysis of the spectral shape*

In order to improve the efficiency of the selection procedure, we have analyzed the shape of the one-dimensional spectra. Each prism spectrum has been characterized by the slopes derived in three bands. Two of them have been chosen at both sides with respect to the point with higher signal, and the last one towards the blue end of the spectrum. Each band covers 10 pixels (about 200 Å) and a second order polynomial fit has been derived for each region. Figure 4 shows the three bands and the fits performed for a typical spectrum. The slopes are calculated in the middle of the blue band ($S1$) and in the pixel of higher signal ($S2, S3$) for the other two bands.

The variations in the slopes will show the distribution and the peculiarities of the prism spectra. In the absence of the Hα line in emission, they will show a smooth instrumental shape, with the two last bands located in the point of higher sensitivity of the IIIaF emulsion. In this case, we expect typical values of $S2 - S1 < 0$ and $S2 - S3 \approx 0$. If the spectrum presents the Hα line in emission, the two last bands will be located on the winds of the line, whereas the first band will show the continuum distribution. The emission line will produce a hard increase in density, high variations in the slope of the continuum and near the line, and strong discontinuities on the top of the line, that is, typical values of $S2 - S1 \gg 0$; $S2 - S3 \gg 0$.

4. Selection of candidates

Candidates of ELGs will be selected to present large differences in the measured parameters with those obtained for the majority of the objects. The criteria will be the existence of high residuals (R) between the extracted spectrum and the estimated continuum, and the presence of strong variations in the slope of the spectrum as exposed in the precedent point. In order to establish the typical values of R, $S2-S1$ and $S2-S3$, we have plotted these parameters versus the density fluxes for each object as shown in Figs. 5a-c. A curve has been fitted to the data following an iterative procedure in order to reject the contribution of points with the largest deviations. The plots show the final fits and the 3σ curve. We compute the difference, in sigma units, between the three measured parameters and those estimated using the fits, filtering the data imposing a minimum of 2σ in each deviation. Finally, we establish a selector index as the sum of these three deviations.

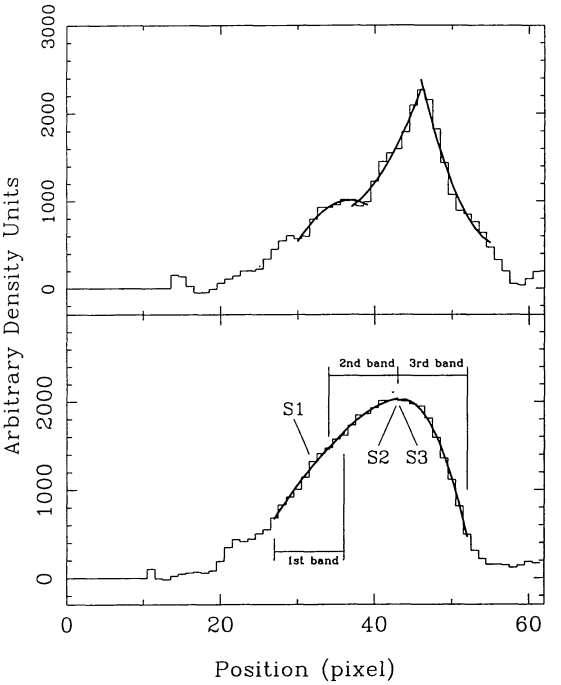

Fig. 4. The shape of the spectra are characterized by the slopes ($S1$, $S2$ & $S3$) derived after a second order polynomial fit in three different bands (see text)

Objects with high emission line features in their prism spectra show deviations larger than 10 sigma with respect to the "normal" values. Nevertheless, it does not exist an abrupt edge between normal and emission line spectra and, in addition, some objects can present a clear line produced by a plate blemish. Therefore, it is necessary to inspect some objects in order to retain a final list of candidates. We have inspected the spectra with a selector index greater than 4, that is, at least spectra with deviation greater than 2 sigma in two criteria or greater than

4 sigma in one of them. It has been necessary to inspect only some tens of objects in a graphic device, where a gray map and the extracted spectrum are available. This procedure provides a considerably reduced subset compared with the nearly $2\,10^4$ initial objects. Spectra showing a strong emission line produced by a plate blemish are easily recognized in the two-dimensional digitized image, and candidates have proved to have the highest values of our priority index. In Fig. 6 we present the prism spectra for the 11 selected candidates, and in Table 2 we show the differences, in sigma units, of the measured parameters R, $S2-S1$ and $S2-S3$, and the final selector index.

Table 2. ELGs candidates

Object Identifier	Log Flux	ΔR σ	$\Delta(S2-S1)\Delta(S2-S3)$ σ	σ	Selector Index
15586	4.792	16.2	12.2	11.7	40.1
2848	4.988	12.2	8.7	13.8	34.7
13394	4.902	4.4	8.6	9.5	22.5
11833	5.106	6.5	6.4	8.1	21.1
17066	4.728	7.8	4.1	5.1	16.9
10877	4.528	4.2	3.8	5.9	13.9
10143	4.503	5.2	0.0	4.9	10.2
9837	4.563	3.6	0.0	5.3	8.9
19406	4.760	0.0	3.9	4.3	8.2
19320	4.720	3.5	0.0	2.6	6.2
16021	4.969	2.1	0.0	3.5	5.6

5. Comparison with the visual sample

In order to test the reliability of the automatic procedure, the prism plate was carefully searched by visually scanning with a low-power binocular microscope by three independent observers, with a last review of all objects to derive a visual sample of candidates. We obtained a final list of 11 candidates. A total of 8 out of 11 candidates are in common with the automatically selected sample. A careful study of the objects missed in both searches enables us to understand the possible fails of the methods. With respect to the objects found only in the visual search:

- NGC 5789 (Sdm; m=14.2; size 0′.9×0′.8), with six visible HII regions, was no paired with their direct image due to its large extension, and, in consequence, not processed.
- NCG 5798 (Im; m=13.6; size 1′.4×1′.0), a bright and irregular galaxy showing five HII regions was lost in the automatic search. The reason is that the extracted prism spectrum concerns the central region of the galaxy, where no emission line is seen. In addition the spectrum is nearly saturated.
- The last remaining object was visually selected but was assigned only as probable candidate because it does not show a clear emission.

On the other hand, the three objects selected only in the automatic search were analyzed:

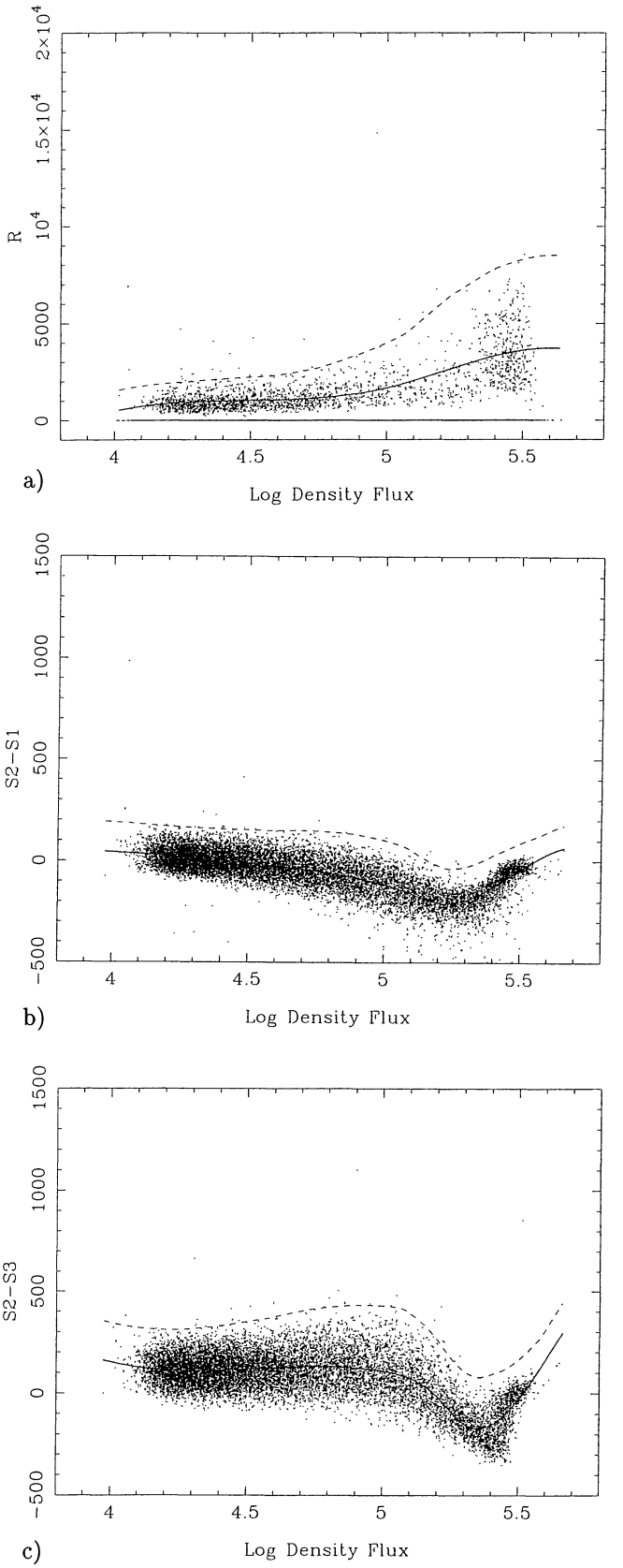

Fig. 5. Dependence of the residua after the continuum fit (R), and the slope variations ($S2-S1$) and ($S2-S3$) with the logarithm of the density fluxes. In each plot we have derived a curve following the general tendency (solid line). Dashed line shows the 3σ deviation curve

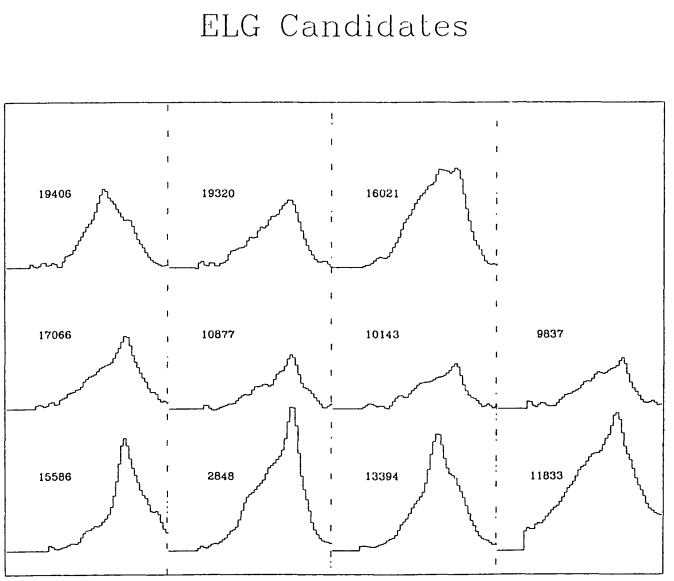

Fig. 6. Prism spectra of the final list of candidates

- #10877 exhibits a clear emission line and it should have been selected, pointing out a fail in the visual procedure.
- #10143 is very faint and its very weak emission-line feature in the digitized spectrum cannot be confirmed in the visual inspection of the plate.
- The emission feature in #19406 is abnormally shifted towards the blue region of the prism spectrum and, in addition, its appearance in the direct plate is stellar-like. It was not visually selected because it presented an anomalous shape, very different to that presented by typical ELG candidates.

So, we can resume that objects with strong lines in emission are not missed in the automatic search. Only bright and large galaxies with extranuclear emitting regions can be lost because of the fail of pairing algorithm or the presence of extranuclear emission. However, their large size and brightness assure them as known galaxies, and they can be recovered in a quick visual scanning of the plate.

6. Spectroscopic observations

The whole sample of 14 candidates selected both visually and automatically, with the exception of the two very bright and known galaxies NGC 5789 and NGC 5798, was observed in July 1994 with the IDS Spectrograph attached to the Cassegrain focus of the Isaac Newton Telescope at La Palma Observatory, Canary Islands, Spain. We used a TEK #3 CCD detector with equivalent pixel size of 24 μm, together with a 300 gr/mm grating, which provides a reciprocal dispersion of 3.3 Å/pixel and a spatial scale of 0.″71/pixel. The wavelength coverage was $\lambda\lambda$ 3600−7100 Å. The slit width was 4″ and the position angle was chosen to match the galaxy mayor axis when some elongated structure was apparent. Exposure times from 300 to 3600 s were taken according to the object brightness. Reduction of data was carried out using the ESO image processing software package (MIDAS), and involves flat-fielding, wavelength calibration, sky subtraction, extinction correction and conversion to absolute flux. The redshifts were measured using the strongest emission lines.

Figure 7 shows the 12 observed objects, together with their prism spectra. The first eight objects (Figs. 7a-h) were identified in both visual and automatic searches. The next three objects (Figs. 7i-k) were detected only in the automatic search, whereas the last one (Fig. 7l) was found only during the visual scan. In Table 3 we list the position, equivalent width and fluxes for the Hα+[NII] blend, the redshift and a preliminary spectral classification according to the visual inspection of the slit spectra. Also we list the designation and magnitudes for known objects, extracted from the NASA/IPAC Extragalactic Database (NED).

The eight objects identified in both searches display, all of them, strong emission lines in their slit spectra, and belong to different types of emission line galaxies. The strong emission line present in the prism spectra permits an easy detection. Two of the objects lost in the visual scan (#10877 & #10143) were confirmed as authentic ELG, whereas #19406 has proved to be a cool late type star with strong molecular bands and Hα in emission. These objects will be recognized in futures searches because they present stellar-like appearance in direct plate and they show the observed excess in the prism spectrum anomaly shifted to the blue part due to the combination of the Hα emission at zero redshift and the strong absorption. Finally, the object presented in Fig. 7l was lost in the automatic search, but spectroscopic observations show #05034 as a normal galaxy without Hα emission. This object was wrongly selected in the visual inspection because its prism spectrum presented a sharp profile.

7. Summary

A fully automatic procedure, developed to select ELGs candidates from the objective-prism plates of the UCM survey, has been presented. A prism plate and a direct plate, used mainly to distinguish between real objects and emulsion scratches, were scanned with the high performance MAMA machine. No density to intensity transformation has been necessary to identify the candidates, although some calibration will be necessary to extend this study and to estimate some physical parameters directly from the plates.

No spectral features are present in the prism spectra due to the reduced spectral range and low dispersion, and only the sharp red cut-off and the Hα line in emission are clearly seen. An automatic continuum fit algorithm has been developed and applied to all the spectra. Candidates are selected to present an anomalous high deviation over

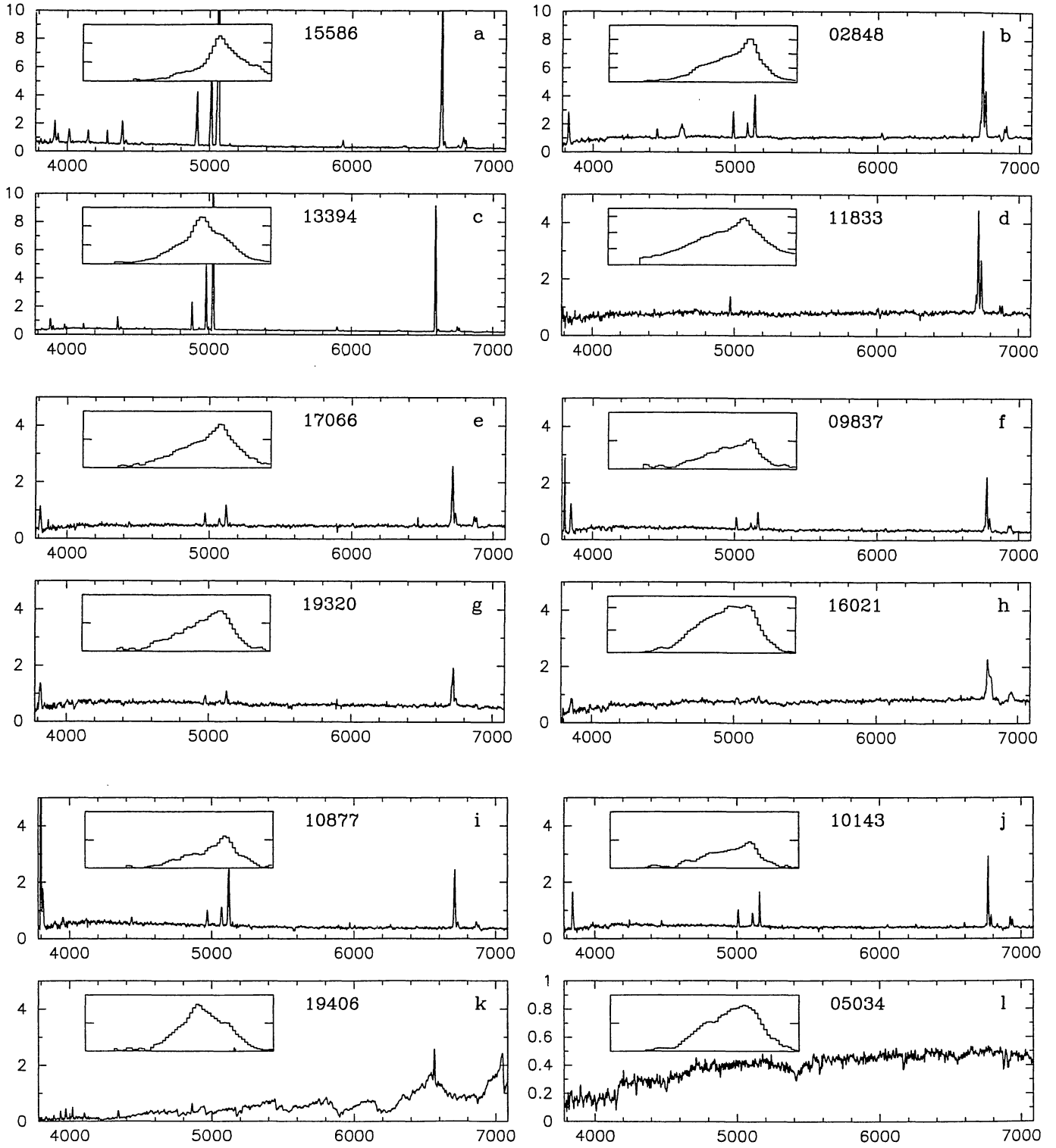

Fig. 7. Slit and prism spectra for the sample of candidates. For each object, the fluxes are given in units of 10^{-15} erg s^{-1} cm^{-2} $Å^{-1}$. Prism spectra cover from 6400 to 6850 Å

Table 3. Spectroscopic data

Object Identifier	(α,δ) (J2000.0)	Hα† Flux‡	EW (Å) Hβ	[OIII]λ5007	Hα†	z	Spectral Type*	Object	m
15586	14 54 12.0 +30 12 34	148.1	105	639	566	0.0107	HIIH	UGC 5988	
2848	15 08 42.6 +28 10 16	130.4	17	28	116	0.0264	HIIH	IRAS 15065+2821	15.3
13394	14 57 39.4 +26 39 53	77.5	50	317	318	0.0047	SS	NPM1G +26.0386	16.2
11833	14 59 34.3 +27 06 58	87.5	6	...	69	0.0226	SBN	UGC 09644	14.2
17066	14 52 22.8 +29 53 26	33.2	10	18	69	0.0225	HIIH	IRAS F14503+3005	
9837	15 00 53.1 +29 43 38	26.7	11	18	82	0.0316	SBN	CG 1277	18.0
19320	14 50 16.3 +28 24 38	24.8	7	8	45	0.0238	SBN		
16021	14 54 22.2 +27 42 04	43.8	5	5	49	0.0334	SBN	IRAS F14522+2754	16.6
10877	15 00 12.3 +28 08 53	27.5	13	48	72	0.0224	HIIH		
10143	15 00 55.6 +27 55 44	26.3	12	24	64	0.0307	HIIH		
19406	14 50 02.4 +27 52 03	...	...	...	...	...	Cool Star		
5034	15 05 33.8 +29 16 07	...	...	...	...	...	No Em.	NPM1G +29.0335	15.5

* According to Salzer et al. (1989). HIIH: HII Hotspot galaxies; SS: Sargent-Searle objects; SBN: Starburst nuclei galaxies.

† Hα fluxes and equivalent widths are referred to as the combined Hα+[NII] emission.

‡ Hα fluxes in units of 10^{-15}erg s^{-1} cm^{-2}

the continuum and/or strong discontinuities in the slopes of the extracted spectra calculated in three bands.

The results presented in the preceding sections demonstrate the consistency of our method against a visual procedure. All the objects detected visually have been recovered, and what is more important, there is a 20% of confirmed emission-line objects only detected through the automatic procedure. Only bright and extended objects with extranuclear HII regions can be lost, but their brightness and size assure them as known galaxies. The uncertainty introduced by wrong identifications (≈20% of plate blemish, scratches or no emission galaxies after a typical visual search; Zamorano et al. 1994) is notably reduced and the amount of beforehand information about each candidate is much bigger, including accurate astrometric positions (error < 1 arcsec).

All these advantages previously mentioned point definitively to the standard implementation of the automatic procedure for analyzing the raw data from Schmidt plates used during emission-line galaxy surveys. It is our intention to extend this work to a greater number of plates of our survey.

Acknowledgements. We would like to gratefully acknowledge the friendly assistance and warm hospitality received from the MAMA staff, and especially from Dr. Jean Guibert. We also express our thanks to the Calar Alto Observatory staff for their inestimable observing support, to M. Cordero, J. Gorgas and S. Pedraz for the first spectroscopic observations of candidates and to A.G. Vitores for useful suggestions and careful review of this paper. This work is based on observations collected at the German- Spanish Astronomical Center, Calar Alto, Spain, operated by the Max-Planck-Institut für Astronomie (MPIA), Heidelberg, jointly with the Spanish National Commission for Astronomy, and with the Isaac Newton Telescope, operated by the Royal Greenwich Observatory at the Spanish Observatory Roque de los Muchachos of the Instituto de Astrofísica de Canarias on behalf of the Science and Engineering Research Council of the United Kingdom and the Netherland Organization for Scientific Research. This work has made use of the NASA/IPAC Extragalactic Database (NED) which is operated by the JET Propulsion Laboratory, Caltech, under contract with the National Aeronautics and Space Administration. This work was supported in part by the Spanish "Programa Sectorial de Promoción General del Conocimiento" under grant No. PB93-456.

References

Birkle K. 1984, The Schmidt Telescope on Calar Alto, ed. Capaccioli, Proc. IAU coll. 78, Astronomy with Schmidt-Type Telescopes (Reidel, Dordrecht) 203

Boroson T.A., Salzer J.J., Trotter A. 1993, ApJ 412, 524

Borra E.F., Brousseau D. 1988, PASP 100, 1276

Borra E.F., Edwards G., Petrucci F. et al. 1987, PASP 99, 535

Clowes R.G., Emerson D., Smith M.G. et al. 1980, MNRAS 193, 415

Edwards G., Beauchemin M., Borra E.F. 1988, PASP 100, 266

Gallego J., Zamorano J., Rego M. et al. 1995, ApJ, in preparation

Guibert J., Moreau O. 1991, The Messenger 64, 69

Haro G. 1956, Bol. Obs. Tonantzintla Tacubaya 14, 8

Hewett P.C., Irwin M.J., Bunclark M.T. et al. 1985, MNRAS 213, 971

Horne K. 1986, PASP 98, 609

Infante L., Pritchet C.J. 1992, ApJS 83, 237

Jarvis J.F., Tyson J.A. 1981, AJ 86, 476

Kennicutt R.C., Kent S.M. 1983, AJ 88, 1094

Kennicutt R.C. 1992, A&A 388, 310

Kinman T.D. 1984, Searching for emission-line galaxies, ed. Capaccioli, Proc. IAU coll. 78, Astronomy with Schmidt-Type Telescopes (Reidel, Dordrecht) 409

Kunth D., Sargent W.L.W. 1986, ApJ 300, 496

Lipovetsky V.A. 1994, The importance of Wide-Field imaging, eds. H.T. MacGillivray et al., Proc IAU Symp. 161, Astronomy from Wide-Field imaging (Kluwer, Dordrecht) 3

MacAlpine G.M., Williams G. 1981, ApJS 45, 113

Markarian B.E. 1967, Astrofizica 3, 55

Markarian B.E., Stepanian J.A., Erastova L.K. 1987, The second Byuracan Spectral Sky Survey, eds. E.Ye. Khachikian et al., Proc. IAU Symp. 121, Observational evidence of activity in galaxies, p. 25

Maza J., Ruiz M.T., González L., Wichnjewsky M. 1989, ApJS 69, 349

Moreau O. 1992, PhD thesis, Université Paris 7

Moss C., Whittle M. 1993, ApJ 407, L17

Moss C., Whittle M., Irwin M.J. 1988, MNRAS 232, 381

Odewahn S.C., Humphreys R.M., Aldering G., Thurmes P. 1993, PASP 105, 1354

Rego M., Zamorano J., González-Riestra R. 1989, A&AS 79, 443

Reid N., Gilmore G. 1982, MNRAS 201, 73

Roeser S., Bastian U. 1991, PPM Star Catalog (Spektrum Akademischer Verlag, Heidelberg, Berlin, New York)

Salzer J.J., MacAlpine G.M., Boroson T.A. 1989, ApJS 70, 479

Schuecker P. 1993, ApJS 84, 39

Smith M.G. 1975, ApJ 202, 591

Surace C., Comte G. 1994, A&A 281, 653

Taff L.G., Lattanzi M.G., Bucciarelli B. 1990, ApJ 358, 359

Takase B., Miyauchi-Isobe N. 1993, Publ. Natl. Astron. Obs. Japan 3, 169

Véron P. 1986, in Structure and Evolution of Active Galactic Nuclei, ed. Guiricin et al. (Reidel, Dordrecht) 253

Wamsteker W., Prieto A., Vitores A.G. et al. 1985, A&AS 62, 255

West R.M. 1991, The Messenger 65, 45

Zamorano J., Rego M., Gallego J., Vitores A.G., González-Riestra R., Rodriguez-Caderot G. 1994, ApJS 95, 387

Zamorano J., Rego M., González-Riestra R., Rodriguez-Caderot G. 1990, Ap&SS 170, 353